Enhancing Gamma Ray Shielding Properties of Oxyanion Complexes: A Comparative Study of CaMoO₄, PbCrO₄, PbMoO₄, and CaWO₄

Nadher Ali Salman, Kafa Khalaf Hammud*

Iraqi Atomic Energy Commission, Iraq

Article information

Abstract

The imperative advancement of gamma-ray shielding materials is pivotal for ensuring radioactive and nuclear safety. In this study, our objective was to ascertain key gamma ray shielding parameters, including the mass attenuation coefficient (μm), effective atomic number (Zeff), half-value layer (HVL), effective electronic density (Neff), mean free path (MFP), and exposure buildup factor (EBF), for four oxyanion complexes (CaMoO₄, PbCrO₄, PbMoO₄, or CaWO₄). These calculations were performed using Phy-X software within the photon interaction range of 0.015-15 MeV. The investigated ternary chromate, tungstate, and molybdate complexes with the molecular formula ABO4, where A = Ca or Pb and B = Mo, Cr, or W, exhibited an exponential decrease in μm with increasing photon energy in the low-energy region. Lead molybdate demonstrated the highest μm followed by PbCrO₄, CaWO₄, and CaMoO₄, correlating with their respective mean atomic numbers and densities. The mean free path values followed the order of PbMoO₄, PbCrO₄, CaWO₄, and CaMoO₄, indicating superior shielding properties due to effective medium-photon interactions. The HVL increased with rising photon energy, with the minimum HVL observed in the presence of lead, primarily attributed to the photoelectric effect. Zeff exhibited a decrease with diminishing mean atomic number and density, with PbMoO₄ displaying the highest Zeff, signifying superior γ-ray shielding capability. The exposure buildup factor (EBF) highlighted the interference of photons by calcium compared to lead compounds. The controlled parameters at low and high energy exposures were attributed to the anion and cation properties of the ternary ABO4, respectively. Among the evaluated materials, PbMoO₄ emerged as the most effective gamma shielding material in the context of nuclear safety.

1. Introduction

Energy and environmental balance becomes more important with respect to pollution and human requirements. For lesser global emissions of warmed gases, nuclear power stations are a renewable energy source that should be installed as the best option in the future. Gamma (γ) rays have two sides in their actions on human health due

to their ionizing nature and high penetration, causing cell mutation and death. Therefore, protection is the first option in this case [1, 2].

The International Radiation Protection Association (IRPA) describes dose limits for workers based on shielding, distance, and time for controlling safety. Shielding is a flexible parameter that provides freedom in material selection, especially in the research sector. Any radiation shielding materials such as lead, iron, copper, tin, alloys, composites, glasses, and biomaterials have wide to limited capability depending on fabrication and cost. Element lead is greatly effective in gamma shielding, but it is toxic, nonrigid, and yields secondary ionized rays. Published papers have suggested many materials for shielding purposes, including aggregation, cracking, strength, moisture photon scattering and other energetic phenomena [2-7].

In radiation and nuclear science and technology, radiation shielding materials are intensively researched and applied in medicine, agriculture, industry, and future generator fusion reactors by looking for materials containing a high atomic number (Z) as a suitable choice for personal protection. In this crucial protection issue, gamma rays, X-rays, and neutrons must be safeguarded to resist cracking, loss of mass (or density) and extraordinary nontransparency properties. One of the most applied materials in this protection section is nontransparent lead element, which has acute and chronic toxicities with anorexia, vomiting, malaise, brain damage, weight loss, weakness, and anemia [8, 9].

Transmission of any ray through a specific medium depends on limitations of Lamberts – Beer Law (Eq. 1) where I: transmitted intensity, I_o: incident intensity, x (cm): thickness of the target, μ (cm^{-1}): Linear Attenuation Coefficient [10].

$$I = I_\circ e^{-\mu x} \quad \ldots\ldots\ldots\ldots \text{ (1)}$$

Gamma rays (γ – rays) can diffuse or penetrate target material as a result of photon (energy) attenuation. With this interaction mechanism, several calculated characters are needed in applied radiation and nuclear science, medicine, engineering, and agriculture. The mass attenuation coefficient (μ_m), effective atomic number (Z_{eff}), half-value layer (HVL), effective electronic density (N_{eff}), mean free path (MFP), and exposure build-up factor (EPF) are numeric characterizations of these ray-material interactions [10, 11].

The latter factor (EPF) in scientific studies [2-12] with high value represents high collision between radiation and the target toward high shielding impact according to its definition "the ratio of total value of specified radiation quantity at any point to the contribution to that value from radiation reaching to the point without having undergone collision".

By using geometrical calculation methods known as geometric progress (G-P) fitting, intensive research papers have recognized metal (with low or high atomic number) behavior towards γ-rays as a computed exposure buildup factor of alloys, glasses, concretes, and others. In many published papers, these numeric characterization factors were calculated by various software programs with or without experimental data [10, 11, 13].

Kolavekara et al. [14] studied several glass systems composed of $47.5P_2O_5 + 45ZnO + (5-x) Bi_2O_3 + 2.5TeO_2 + xSm_2O_3$ with density range (3.02 – 3.70) by Phy-X/PSD software by penetration depths: (1–40) MFP, materials in mol%: Sm_2O_3: 0.01 – 1; P_2O_5: 47.50; ZnO: 45.00; TeO_2: 2.50; Bi_2O_3: 4-5; and thickness (mm): 1.84 – 2.08. They found several important points:

➢ The mass attenuation coefficient decreased with increasing photon energy [(0.015 – 15) MeV] in the absence of Sm_2O_3 addition.
➢ Z_{eq} values were lower at 100 keV and energy (1–15) MeV due to the presence of Compton scattering.
➢ Exposure and energy absorption buildup factors were smaller in both energy regions as photoabsorption and pair creation processes.
➢ A 1% mole Sm_2O_3 showed higher exposure buildup and energy absorption buildup values in the intermediate energy region.

➢ Density, EAN, and transparency to visible light confirmed the use of these glasses as shielding materials in nuclear reactors and technologies.

Additionally, the Iraqi group guided by Taqi [15] published a study about "xPbO, (80-x) B_2O_3, 20Na_2O where (x=0, 10, 20, 30, 40, and 50)". Other experimental conditions were NaI(Tl) detector; Photon energies: (511, 662, and 1173) keV of [22]Na, ^{137}Cs, and ^{60}Co, respectively; Collimators: 3 mm to absorb narrow beam of γ-rays. System shielding: 5 cm lead, 0.5 cm copper, and 0.5 cm steel walls. System background: 900 s; lead borate glass system doped with sodium: melt-quenching technique. Calculated μm, HVL, MFP, Z_{eff}, N_{eff}, and others by WinXCom and Phy-X/PSD computer programs compared to experimental data were in the energy range (1 keV to 1 GeV). Their results revealed remarkable notes:

➢ μ_m decreased with increasing energy due to glass-radiation interactions with photoelectric, Compton scattering, and pair production at low, intermediate, and high energies, respectively. Additionally, μ_m improved as PbO increased.
➢ HVL values tend to increase with PbO lowering or density [(2.175 – 5.213) gm/cm^3].
➢ The calculated results showed a decrease in cross-sections with the incident photon energy, which was improved by the presence of PbO due to photoelectric, pair production, and Compton effects.
➢ Z_{eff} and N_{eff} were influenced by energy and PbO concentration.
➢ The γ-ray absorbance in this study was improved by a higher Z occurrence, such as lead (Pb), in the glass network, as in other studied glass systems, such as $PbO-SiO_2$, $Bi_2O_3-BaO-PbO$, $PbO-Li_2O-B_2O_3$, and $PbO-WO_3-TeO_2$.

Bismuth tungstate ($Bi_2(WO_4)_3$)/((5, 10, 15, and 20) %) was added by Yilmaz and Akman [16] into polymeric composites consisting of unsaturated polyester resin and cobalt octoate (6%), in addition to methyl ethyl ketone peroxide, to explore their performance as gamma shielding. Twenty-two energies from [22]Na, [54]Mn, [57]Co, ^{60}Co, [133]Ba, ^{137}Cs, [152]Eu and [241]Am with the HPGe detector and energy range (59.5-1408.0) keV as experimental factors were compared with theoretical calculations. The resulting polymeric composites in this study and others [17-19] led to innovative areas of research in concrete, paint, elastomers, and others in industry, engineering, agriculture, etc.

According to our knowledge, tungstate and other oxyanion complexes related to Group 6, as a part of the natural transition elements in the periodic table, contain chromium ($_{24}$Cr), molybdenum ($_{42}$Mo), and tungsten ($_{74}$W) and have not been studied as gamma shielding materials without being a part of a network formula.

In general, these metals have extreme mechanical resistance (wear and heat). Calcium molybdate (VI) ($CaMoO_4$), lead chromate (VI) ($PbCrO_4$), lead molybdate (VI) ($PbMoO_4$), and calcium tungstate (VI) ($CaWO_4$) are examples of oxyanion complexes having group (6) ions with the highest oxidation state [molybdenum (Mo^{6+}), chromium (Cr^{6+}) or tungsten (W^{6+})] as hexavalent $O^-M^{6+}(=O)_2-O^-$.

Known structural, physical, chemical, and mechanical properties of calcium molybdate (VI) ($CaMoO_4$), lead chromate (VI) ($PbCrO_4$), lead molybdate (VI) ($PbMoO_4$), and calcium tungstate (VI) ($CaWO_4$) were our bases to choose as tested materials for gamma shielding through theoretical calculations of the mass attenuation coefficient (μ_m), effective atomic number (Z_{eff}), half-value layer (HVL), effective electronic density (N_{eff}), mean free path (MFP), and exposure buildup factor (EPF) in a wide energy range. These major γ-ray parameters were calculated by the Phy-X/PSD computer program.

2. Experimental section
Four oxyanion complexes named calcium molybdate (VI) ($CaMoO_4$), lead chromate (VI) ($PbCrO_4$), lead molybdate (VI) ($PbMoO_4$), and calcium tungstate (VI) ($CaWO_4$) and coded S1, S2, S3, and S4, respectively, are shown in Table (1).

Table (1): General specifications of the tested materials.

Code	Chemical formula, Molecular weight	Density, gm/cm³	Percentage Composition, %		Mean Atomic Number, $\bar{Z}$
S1	$CaWO_4$, 287.92	6.06	Ca	13.92	**21.00**
			O	22.23	
			W	63.85	
S2	$CaMoO_4$, 200.02	4.35	Ca	20.04	**15.66**
			Mo	47.97	
			O	32.00	
S3	$PbMoO_4$, 367.14	6.92	Mo	26.13	**26.00**
			Pb	56.44	
			O	17.43	
S4	$PbCrO_4$, 323.19	6.3	Cr	16.09	**23.00**
			Pb	64.11	
			O	19.80	

3. Theoretical Part

This Various theoretical parameters that can be calculated by Phy-X software include the average molecular weight (AMW), mass attenuation coefficient (MAC), linear attenuation coefficient (LAC), half value layer (HVL), tenth value layer (TVL), mean free path (MFP), atomic cross section (ACS), electronic cross section (ECS), effective atomic number (Zeff), effective electron density (Neff), effective conductivity (Ceff), ratio $(\mu/\rho)com/(\mu/\rho)total$, equivalent atomic number (Z_{eq}), G-P fitting parameters for EBF (GPEBF), G-P fitting parameters for EABF (GPEABF), EBF as a function of MEP (EBF), EABF as a function of MFP, and fast neutron removal cross section (FNRCS). The studied parameters in this study represented by their semi-empirical equations (Table 2) were chosen and discussed for each sample (Figures 1 -4).

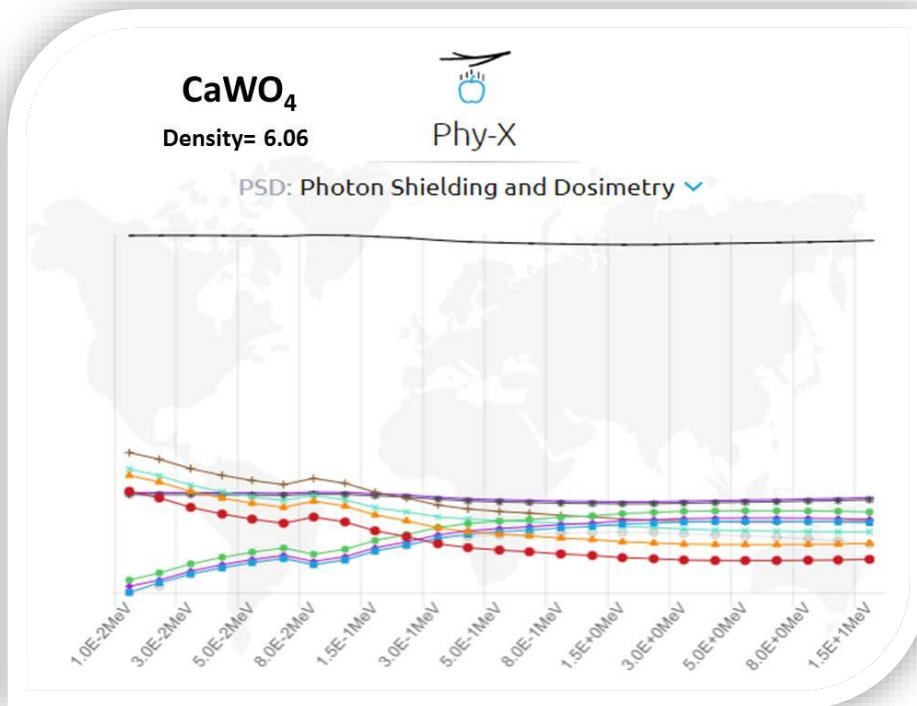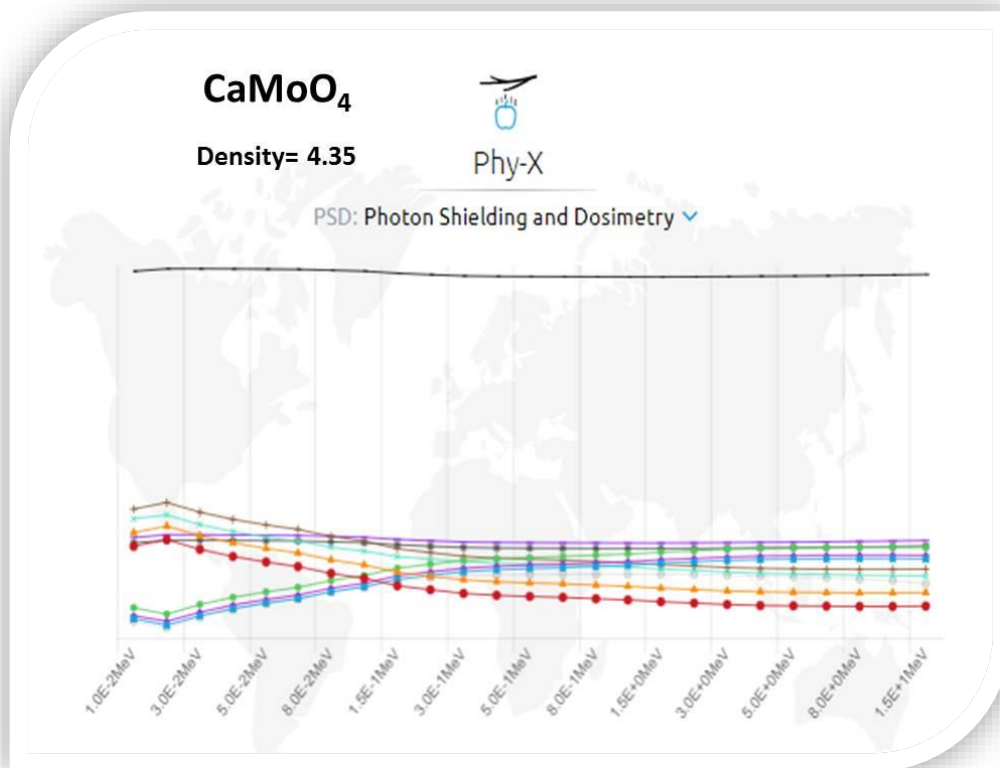**Figure (1):** Calcium tungstate chart by Phy-X online software.

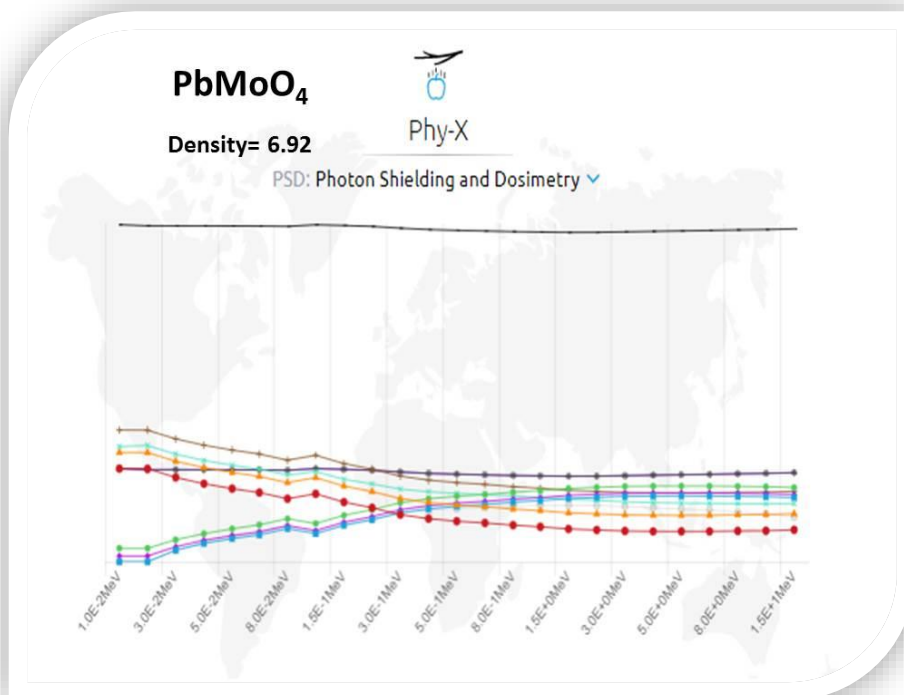**Figure (2):** Calcium molybdate chart by Phy-X online software.

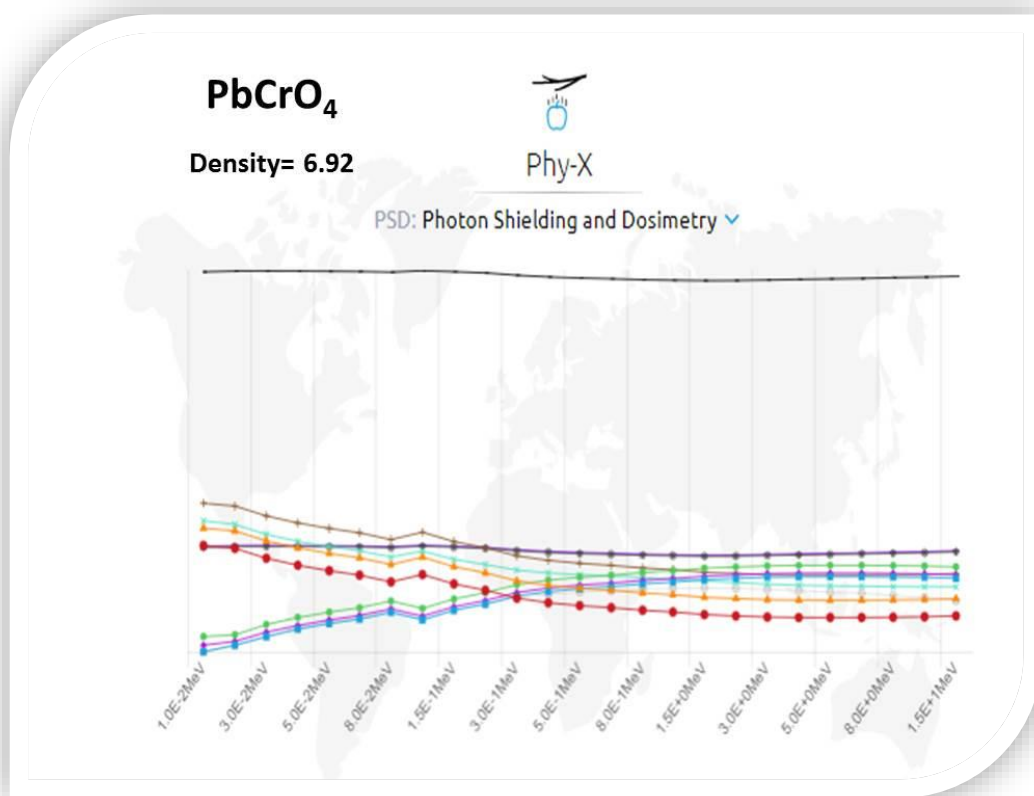**Figure (3):** Lead molybdate chart by Phy-X online software.

Figure (4): Lead chromate chart by Phy-X online software.

Table (2): The semi-empirical equations of the calculated parameters.

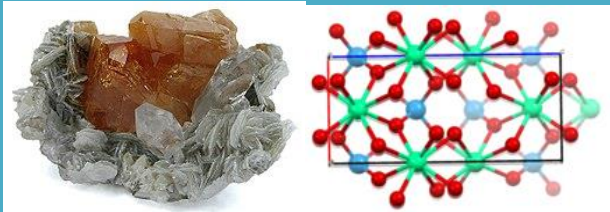| Calculated parameter	Representative equation	Equation identifiers
Mass Attenuation Coefficient μ_m	$$\mu_m = \sum_i^n w_i (\mu/\rho)_i$$	w_i: weight fraction as $w_i = \dfrac{n_i A_i}{\sum_i n_i A_i}$ A_i : atomic weight n_i : formula units
Effective Atomic Number Z_{eff}	$$Z_{eff} = \frac{\sigma_a}{\sigma_e}$$ $$\sigma_t = \frac{\mu_m M}{N_A}$$ $$\sigma_a = \frac{1}{N_A}\sum f_i A_i \left(\frac{\mu}{\rho}\right)_i$$ $$\sigma_e = \frac{1}{N_A}\sum f_i \frac{A_i}{Z_i}\left(\frac{\mu}{\rho}\right)_i$$ $$\sigma_e = \frac{\sigma_a}{Z_{eff}}$$	$M = \sum_i^n n_i A_i$ is the molecular weight N_A : Avogadro number Effective atomic cross- section σ_a Total electronic cross-section σ_e **Fractional abundance**: $f_i = \dfrac{n}{\sum_i n_i}$ $$\sum_i^n f_i = 1$$ Z_i: atomic number
Effective Electronic Density N_{eff}	$$N_{eff} = N_A \frac{n Z_{eff}}{\sum_i n_i A_i}$$ $$= N_A \frac{Z_{eff}}{A}$$	A: mean atomic mass
Half Value Layer HVL Effectiveness of gamma –ray shielding as "the thickness of the material that reduces the photon beam intensity to the half of its initial value (I_o)"	$$HVL = \frac{0.693}{\mu}$$	μ: Linear Attenuation Coefficient
Mean Free Path MFP "the average distance between two successive interaction of photons"	$$MFP = \frac{1}{\mu}$$	μ: Linear Attenuation Coefficient
Exposure Buildup Factor (EBF): Buildup factor as "the ratio of the total detector response to that of uncollided photons", may refer to total exposed photons by the target material to the total noninterfered photons due to multiple photon – material interaction phenomena like Compton Scattering	logarithmic interpolation: $(\mu/\rho)_{compton}/(\mu/\rho)_{Total}$ as Z_{eq} G-P fitting parameters and buildup factor $$B(E,X) = 1 + \frac{b-1}{k-1}(k^X - 1) \text{ for } k \neq 1$$ $$B(E,X) = 1 + (b-1)X \text{ for } k = 1$$ $$k(E,X)$$ $$= cX^a + d\frac{\tanh(X/X_g) - \tanh(-2)}{1 - \tanh(-2)}$$	E: energy , X: penetration depth B: buildup factor at 1 mfp, $k(E, x)$: dose multiplicative factor

4. Results and Discussion

Gamma ray properties are specified according to their frequency ($>10^{19}$ Hz), energy (>100 KeV), and wavelength (<10 pm), where atomic nuclei energy release is produced from the high-energy orbit to the intermediate and then to the lower stage as two transition states. These high-energy penetrating rays are defined as very dangerous to all living creatures after exposure and can be scattered or absorbed by various shielding materials for safety, especially in the laboratory, industry, and locations containing naturally occurring radioactive materials (NORM), such as oil wells and related petroleum industries [14, 15, 16, 20, 21, 22]. Protection of individuals and infrastructure from γ-radiation, in particular friendly based shielding materials, which is based on many chemical and structural properties [20, 21, 22, 23].

Many Iraqi researchers were a part of the scientific community in γ-ray shielding through thesis and research articles where theoretical and experimental studies were performed [15, 24, 25, 26, 27, 28, 29]. The tested oxyanion complexes have important properties that can provide good support in addition to the resulting data. These materials vary in their major characteristics as shown in Table 3. The key characteristics are their high

melting point and insolubility in water, which is a significant property for environmental concerns. According to scientific references [30, 31], tungstate and molybdate have tetragonal structures, and this scheelite structural type presents unique uses in light emitting diodes, photocatalysis, scintillation, optical filters, and other technologies. For example, calcium tungstate configurations of tungsten atoms are surrounded by oxygen atoms with tetrahedral symmetry, and calcium is surrounded by eight oxygen atoms with octahedral symmetry. Tested oxyanions as γ-ray shields have been explored through important factors abbreviated as (μ_m, Z_{eff}, N_{eff}, HVL, MFP, and EBF) with incident photons in the energy range of 0.015 – 15 MeV (Figures (1-4)).

Table (3): Several characteristics of the tested oxyanion complexes.

Formula	Characteristics
$CaWO_4$	Occurrence: scheelite. Properties: Tetragonal crystals. Solubility: Practically insoluble in water. Melting point: (1570 – 1670)ºC. Applications: diagnosis of malignant tumours, paints, scintillation counters.
$CaMoO_4$	Powellite as its mineral with tetragonal – dipyramidal as transparent adamantine with colour range from blue to grey. Property: Tetragonal crystals. Melting point: 965ºC. Solubility: Practically insoluble in water. Applications: Phosphors and luminescent materials.
$PbMoO_4$	Wulfenite as its mineral found as thin tabular crystals in tetragonal system. Colour: Yellow powder. Solubility: Insoluble in water. Applications: pigments.
$PbCrO_4$	Presence of lead ion distorted coordination sphere of the oxyanion where it is surrounded by Pb-O (2.53 - 2.80) Å giving tetrahedral structure with orthorhombic and monoclinic forms. It occurs in nature as phoenicochroite and crocoite. Colour: Yellow or orange–yellow powder. Melting point: 844ºC. Solubility: insoluble salts (0.2 mg/L water). Toxicity: highly toxic and carcinogen. LD_{75} i.p. in guinea pigs: 156 mg/kg. Applications: Pigment in oil, printing fabrics, porcelain; chemical analysis, and traffic paints.

The mass attenuation coefficients decreased exponentially with increasing photon energy (93.236, 79.249, 70.745, and 20.245) in the low-energy region and then sharply decreased. Lead molybdate $PbMoO_4$ had the highest(μ_m) value, followed by $PbCrO_4$, $CaWO_4$, and $CaMoO_4$, which was related to the decrease in mean atomic numbers and densities (Table 4).

The mean free path (MFP) values decreased in the order of PbMoO$_4$, PbCrO$_4$, CaWO$_4$, and CaMoO$_4$ in the reverse μm results, where the MFP did not depend on the density. For that, PbMoO$_4$, which has the highest density, presented the lowest density due to the interaction between photons and the medium, indicating superior shielding properties. Increasing energy led to an increase in the MFP of all four samples (Table 4, Figures (1-5)).
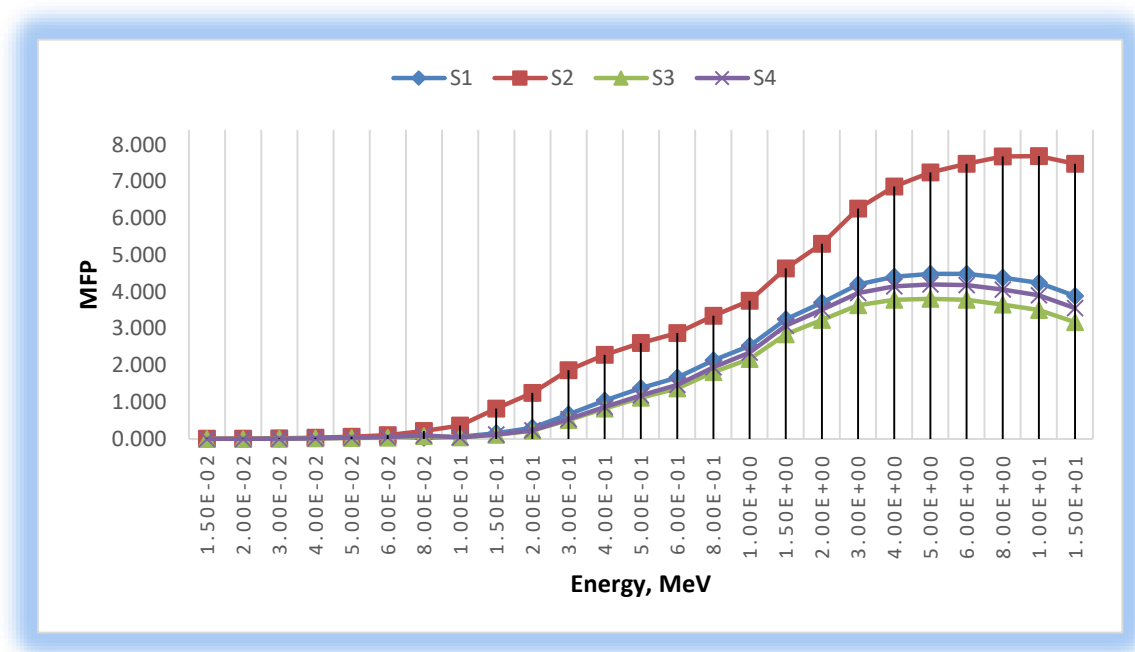

Figure (5): Change in the mean free path with energy for all four samples.

Table (4): Results of mass attenuation coefficients and mean free path (MFP) according to their energy values.

Energy, MeV	Mass Attenuation Coefficient (μ$_m$, cm^2/gm)				Mean Free Path (MFP, cm)			
	S1	S2	S3	S4	S1	S2	S3	S4
1.50E-02	93.236	20.245	70.745	79.249	0.002	0.011	0.002	0.002
2.00E-02	43.974	41.049	69.684	58.825	0.004	0.006	0.002	0.003
3.00E-02	15.165	14.416	24.518	20.546	0.011	0.016	0.006	0.008
4.00E-02	7.125	6.656	11.530	9.717	0.023	0.035	0.013	0.016
5.00E-02	3.989	3.649	6.415	5.447	0.041	0.063	0.023	0.029
6.00E-02	2.505	2.243	3.983	3.411	0.066	0.103	0.036	0.047
8.00E-02	5.074	1.068	1.907	1.663	0.033	0.215	0.076	0.095
1.00E-01	2.903	0.627	3.445	3.639	0.057	0.367	0.042	0.044
1.50E-01	1.063	0.279	1.271	1.347	0.155	0.824	0.114	0.118
2.00E-01	0.548	0.183	0.648	0.687	0.301	1.254	0.223	0.231
3.00E-01	0.246	0.123	0.282	0.297	0.671	1.873	0.512	0.535
4.00E-01	0.158	0.100	0.175	0.183	1.046	2.289	0.825	0.869
5.00E-01	0.120	0.088	0.129	0.134	1.378	2.609	1.117	1.184
6.00E-01	0.099	0.080	0.105	0.108	1.666	2.881	1.376	1.467
8.00E-01	0.077	0.069	0.080	0.082	2.138	3.346	1.813	1.946
1.00E+00	0.065	0.061	0.066	0.068	2.527	3.757	2.175	2.345
1.50E+00	0.051	0.050	0.051	0.052	3.255	4.632	2.843	3.081

Energy, MeV	Mass Attenuation Coefficient (μ_m, cm^2/gm)				Mean Free Path (MFP, cm)			
	S1	S2	S3	S4	S1	S2	S3	S4
2.00E+00	0.045	0.043	0.045	0.045	3.707	5.309	3.236	3.516
3.00E+00	0.039	0.037	0.040	0.040	4.202	6.262	3.634	3.969
4.00E+00	0.037	0.033	0.038	0.038	4.413	6.864	3.780	4.149
5.00E+00	0.037	0.032	0.038	0.038	4.486	7.244	3.809	4.199
6.00E+00	0.037	0.031	0.038	0.038	4.486	7.477	3.781	4.181
8.00E+00	0.038	0.030	0.040	0.039	4.387	7.679	3.655	4.063
1.00E+01	0.039	0.030	0.041	0.041	4.241	7.694	3.504	3.909
1.50E+01	0.042	0.031	0.046	0.045	3.885	7.479	3.171	3.554

In general, the half value layer (HVL) describes radiation attenuation where a good shielding material has a lower HVL. In this theoretical study, the HVL values of all samples increased with increasing incident photon energy from 0.015 MeV to 15 MeV (Table 5, Figures 1-4). Additionally, the minimum HVL was detected with the presence of lead (Pb) in PbMoO$_4$ and PbCrO$_4$, while the maximum value had the lowest atomic number (calcium Ca) in CaMoO$_4$ and CaWO$_4$ due to the photoelectric effect that depends on the atomic number (Z) or mean atomic number ($\overline{Z}$), where $\overline{Z}$ of PbMoO$_4$ and PbCrO$_4$ are 26 and 23, respectively (Table 1).

Effective atomic number (Z_{eff}) and effective electronic density (N_{eff}) calculated with the assistance of the mass attenuation coefficients of each sample as mentioned in Table 2 in the energy range (0.015 to 15) MeV.

As is known in published research, the effective atomic number differs with energy. This note was observed in this work in addition to decreasing Z_{eff} with decreasing mean atomic number and density. Z_{eff} values began to rise with energy change until reaching a maximum value at 80, 30, 71, and 100 KeV for CaWO$_4$, CaMoO$_4$, PbMoO$_4$, and PbCrO$_4$, respectively. This rise gradually decreased and then became nearly constant at high photon energies due to the effect of the atomic number (Z) on the probability of material-photon interactions known as photoelectric, Compton, and pair production. Additionally, the Z_{eff} of PbMoO$_4$ was the highest among the oxyanion complexes, indicating the highest γ-ray shielding capability.

By gamma rays beam falling on the tested sample, photonic interactions occurred as an absorption and scattering that varied according to the energy and atomic number. From these interactions, secondary photons are produced, leading to a rise in photon fluidity. All photon–material interactions can be summarized by a dimensionless factor called exposure buildup factor EBF, where calculation steps begin from the equivalent atomic number (Z_{eq}) as a relation between Compton mass attenuation and the total attenuation at a defined energy and then Geometric Progression (G-P) fitting parameters (b, c, a, X_k, d) in the applied energy range (Table 6).
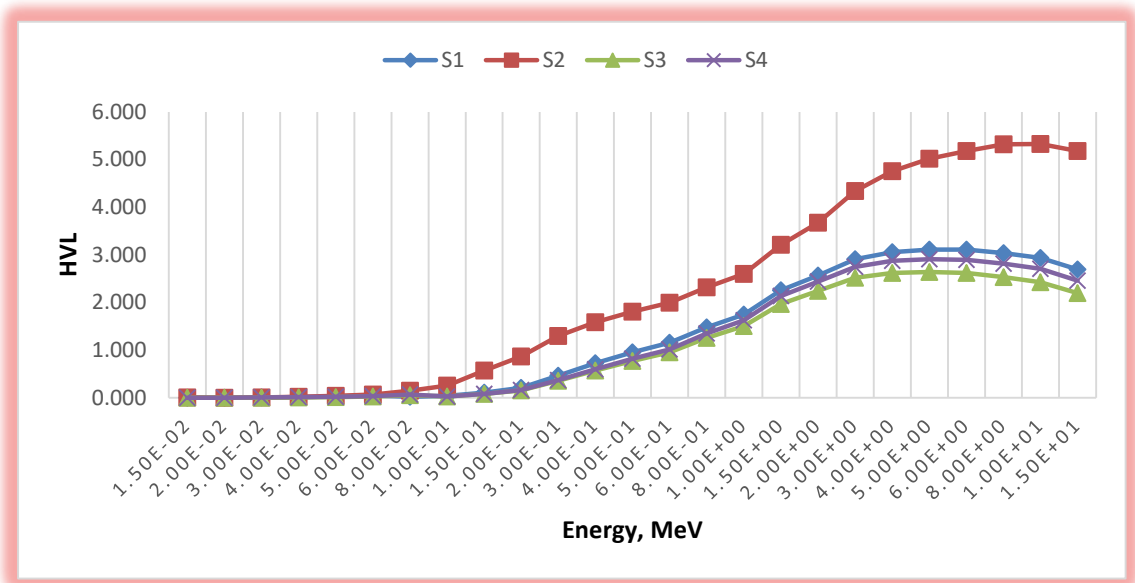
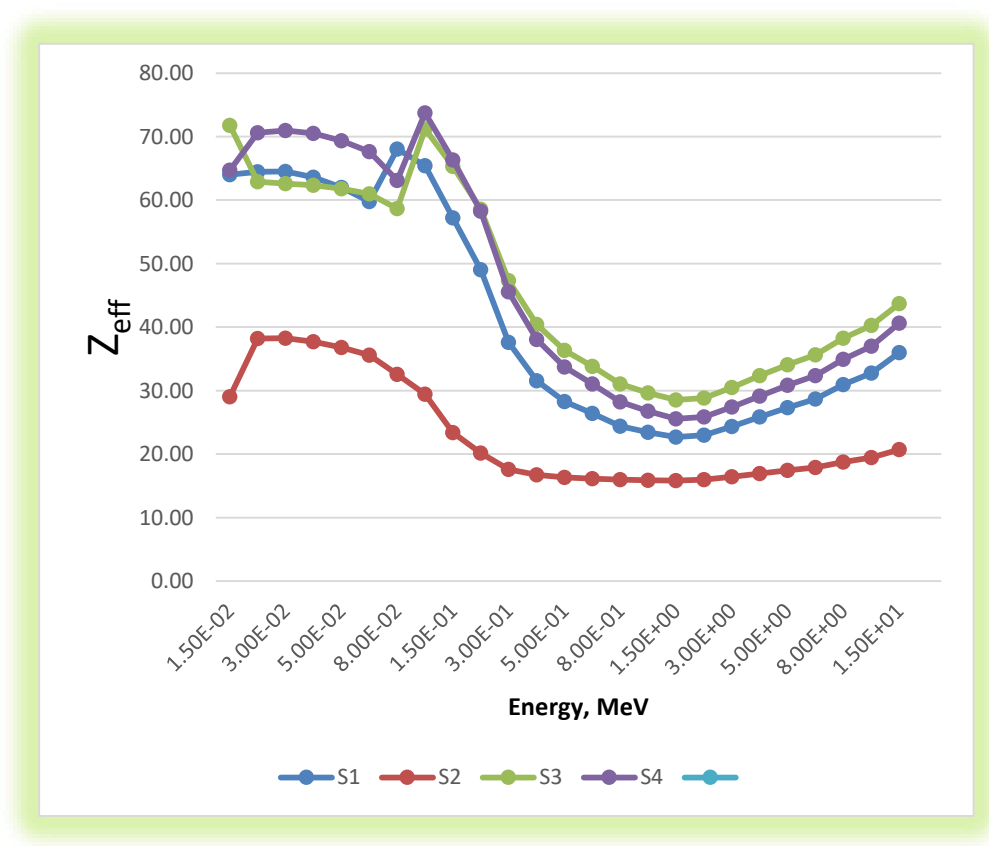**Figure (6):** Change in the Half Value Layer with energy for all four samples.

Figure (7): Changes in the effective atomic number with energy for all four samples.
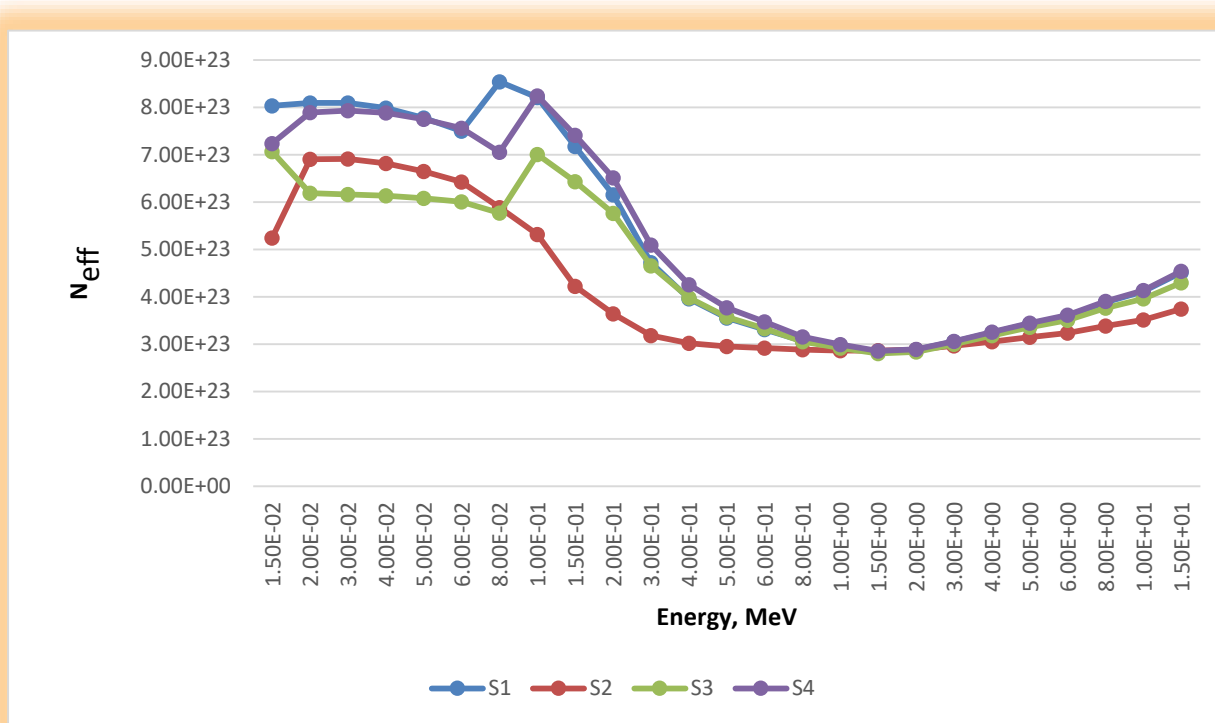
Figure (8): Changing of Effective Electronic Density with energy for all four samples.

Table (5): Results of Half Value Layer (HVL) Effective atomic number (Z_{eff}) and Effective Electronic Density (N_{eff}) according to their energy values.

Energy, MeV	HVL, cm⁻¹				Z_{eff}				N_{eff} (E+23)			
	S1	S2	S3	S4	S1	S2	S3	S4	S1	S2	S3	S4
1.50E-02	0.001	0.008	0.001	0.001	64.00	29.01	71.79	64.73	8.03	5.24	7.07	7.24
2.00E-02	0.003	0.004	0.001	0.002	64.48	38.22	62.88	70.59	8.09	6.91	6.19	7.89
3.00E-02	0.008	0.011	0.004	0.005	64.53	38.25	62.59	70.97	8.10	6.91	6.16	7.93
4.00E-02	0.016	0.024	0.009	0.011	63.62	37.72	62.34	70.51	7.98	6.81	6.14	7.88
5.00E-02	0.029	0.044	0.016	0.020	61.97	36.81	61.81	69.35	7.78	6.65	6.08	7.75
6.00E-02	0.046	0.071	0.025	0.032	59.76	35.58	61.00	67.64	7.50	6.43	6.00	7.56
8.00E-02	0.023	0.149	0.053	0.066	68.03	32.58	58.66	63.10	8.54	5.89	5.77	7.05
1.00E-01	0.039	0.254	0.029	0.030	65.41	29.43	71.19	73.75	8.21	5.32	7.01	8.24
1.50E-01	0.108	0.571	0.079	0.082	57.19	23.39	65.33	66.31	7.18	4.23	6.43	7.41
2.00E-01	0.209	0.869	0.154	0.160	49.05	20.17	58.55	58.25	6.16	3.64	5.76	6.51
3.00E-01	0.465	1.298	0.355	0.371	37.61	17.60	47.32	45.56	4.72	3.18	4.66	5.09
4.00E-01	0.725	1.586	0.572	0.602	31.56	16.73	40.40	38.05	3.96	3.02	3.98	4.25
5.00E-01	0.955	1.809	0.774	0.821	28.30	16.35	36.32	33.70	3.55	2.95	3.57	3.77
6.00E-01	1.155	1.997	0.954	1.017	26.40	16.15	33.81	31.07	3.31	2.92	3.33	3.47
8.00E-01	1.482	2.320	1.257	1.349	24.42	15.96	31.06	28.20	3.06	2.88	3.06	3.15
1.00E+00	1.751	2.604	1.508	1.625	23.44	15.87	29.66	26.76	2.94	2.87	2.92	2.99
1.50E+00	2.256	3.210	1.971	2.135	22.69	15.84	28.51	25.56	2.85	2.86	2.81	2.86

Energy, MeV	HVL, cm^{-1}				Z_{eff}				N_{eff} (E+23)			
	S1	S2	S3	S4	S1	S2	S3	S4	S1	S2	S3	S4
2.00E+00	2.569	3.680	2.243	2.437	22.99	15.97	28.85	25.85	2.88	2.88	2.84	2.89
3.00E+00	2.912	4.341	2.519	2.751	24.33	16.41	30.50	27.40	3.05	2.96	3.00	3.06
4.00E+00	3.059	4.758	2.620	2.876	25.86	16.92	32.35	29.15	3.25	3.06	3.18	3.26
5.00E+00	3.109	5.021	2.640	2.910	27.32	17.43	34.08	30.83	3.43	3.15	3.35	3.45
6.00E+00	3.110	5.182	2.621	2.898	28.65	17.90	35.64	32.36	3.60	3.23	3.51	3.62
8.00E+00	3.041	5.323	2.534	2.816	30.93	18.74	38.23	34.94	3.88	3.39	3.76	3.91
1.00E+01	2.940	5.333	2.429	2.710	32.76	19.44	40.26	37.01	4.11	3.51	3.96	4.14
1.50E+01	2.693	5.184	2.198	2.463	35.98	20.70	43.68	40.61	4.52	3.74	4.30	4.54

Table (6a): G-P fitting parameters (a, b, c, d, X_k) of the tested oxyanion complexes.

a	b	c	d	X_k	a	b	c	d	X_k
CaWO4					CaMoO$_4$				
-0.154	1.003	1.552	0.146	11.581	0.142	1.009	0.494	-0.284	29.254
0.523	1.512	0.728	-0.721	11.599	0.405	1.025	0.389	-0.466	13.093
0.170	1.974	0.626	-0.112	19.325	0.221	1.110	0.507	-0.166	14.401
0.179	2.189	0.327	-0.071	17.979	0.176	1.143	0.375	-0.232	24.928
0.007	1.931	0.220	-0.058	12.497	0.139	1.153	0.274	-0.072	11.684
0.622	1.687	0.204	-0.141	15.311	0.406	1.179	0.250	-0.162	14.638
-0.003	2.067	0.338	-0.027	16.231	0.328	1.263	0.297	-0.155	14.281
0.356	1.537	0.131	-0.063	16.683	0.197	1.319	0.445	-0.114	17.560
0.429	1.196	0.183	-0.239	13.795	0.236	1.878	0.418	-0.145	13.722
0.219	1.170	0.407	-0.117	14.186	0.195	2.481	0.534	-0.133	13.668
0.141	1.248	0.551	-0.065	13.816	0.086	2.713	0.778	-0.068	13.297
0.097	1.335	0.676	-0.053	14.214	0.044	2.748	0.926	-0.055	12.886
0.074	1.405	0.751	-0.044	14.144	0.016	2.647	1.023	-0.038	12.522
0.056	1.450	0.806	-0.035	13.755	0.003	2.551	1.067	-0.031	11.994
0.037	1.511	0.876	-0.028	13.688	-0.009	2.368	1.108	-0.024	10.831
0.023	1.531	0.931	-0.022	13.504	-0.015	2.230	1.123	-0.018	9.825
0.001	1.503	1.032	-0.016	13.943	-0.021	1.949	1.134	-0.010	9.629
0.002	1.529	1.043	-0.021	13.109	-0.019	1.835	1.113	-0.005	9.581
0.014	1.536	1.026	-0.041	13.249	0.002	1.681	1.037	-0.018	12.396
0.021	1.481	1.021	-0.048	13.497	0.014	1.563	0.998	-0.030	13.961
0.046	1.491	0.957	-0.073	13.687	0.024	1.476	0.969	-0.038	14.144
0.059	1.482	0.931	-0.084	13.905	0.023	1.396	0.976	-0.038	14.271
0.077	1.527	0.903	-0.098	14.157	0.033	1.301	0.956	-0.044	13.877
0.052	1.503	1.007	-0.074	14.191	0.038	1.238	0.953	-0.049	14.238
0.030	1.584	1.167	-0.058	14.022	0.046	1.150	0.955	-0.052	14.615

Table (6b): G-P fitting parameters (a, b, c, d, X_k) of the tested oxyanion complexes.

a	b	c	d	X_k	a	b	c	d	X_k
		$PbMoO_4$					$PbCrO_4$		
-0.253	1.002	1.857	0.214	11.511	-0.216	1.002	1.736	0.190	11.744
0.069	1.201	1.833	-0.067	17.494	0.163	1.152	1.431	-0.178	16.268
0.120	1.465	1.029	-0.125	26.373	0.148	1.365	0.882	-0.136	23.004
0.114	1.452	0.326	-0.065	23.402	0.131	1.367	0.339	-0.111	23.822
-0.128	1.362	0.072	0.104	8.604	-0.057	1.307	0.125	0.058	9.419
0.770	1.316	0.040	-0.189	14.890	0.678	1.281	0.093	-0.182	14.826
0.563	1.298	0.090	-0.225	14.050	0.508	1.290	0.139	-0.209	14.104
0.012	1.659	0.303	0.034	18.138	0.033	1.676	0.373	0.011	17.900
0.588	1.498	0.072	-0.240	16.542	0.539	1.515	0.078	-0.200	17.929
0.532	1.496	0.122	-0.278	13.820	0.553	1.502	0.112	-0.283	13.847
0.348	1.618	0.253	-0.194	13.352	0.360	1.603	0.241	-0.200	13.341
0.264	1.789	0.373	-0.169	13.749	0.273	1.758	0.360	-0.173	13.738
0.210	1.912	0.466	-0.139	13.797	0.217	1.877	0.452	-0.143	13.780
0.152	1.845	0.575	-0.100	13.620	0.156	1.805	0.563	-0.102	13.607
0.115	1.942	0.667	-0.081	13.589	0.119	1.907	0.654	-0.082	13.586
0.093	1.963	0.729	-0.072	13.521	0.097	1.933	0.717	-0.073	13.524
0.052	1.848	0.868	-0.054	13.759	0.054	1.830	0.861	-0.055	13.784
0.061	1.856	0.860	-0.069	13.387	0.062	1.842	0.857	-0.069	13.395
0.093	1.827	0.802	-0.111	13.517	0.093	1.825	0.802	-0.111	13.517
0.109	1.759	0.773	-0.127	13.855	0.110	1.772	0.771	-0.127	13.853
0.145	1.853	0.701	-0.159	14.108	0.137	1.811	0.718	-0.153	14.077
0.140	1.778	0.722	-0.153	14.246	0.133	1.724	0.738	-0.148	14.216
0.124	1.774	0.787	-0.140	14.298	0.120	1.677	0.795	-0.137	14.312
0.086	1.700	0.924	-0.108	14.152	0.086	1.581	0.920	-0.106	14.210
0.054	1.704	1.117	-0.087	13.928	0.057	1.545	1.098	-0.088	14.017

As mentioned in Table 2, the exposure buildup factor (EBF) can be considered as the ratio of total photons interfered by the objective to the total noncollided photons, giving a numeric absorbed energy of photon – material interactions such as Compton scattering, photoelectric, and/or pair production.

Varied EBF values for all four materials began at 1.50E-02 MeV as a starting point, whereas chemical composition is a major director in all tested characters, exclusively EBF, as summarized below:

❖ Calcium compounds ($CaMoO_4$ and $CaWO_4$) gave one stage of change in the shape of the peak followed by an approximately similar quantity, while lead compounds ($PbCrO_4$ and $PbMoO_4$) gave two stages of change.
❖ In calcium compounds, the presence of tungsten in the oxyanion presented a higher EBF value at higher energy compared to the molybdenum oxyanion complex, where tungsten has a higher atomic number (or mass) than molybdenum in addition to variation in density (Table 1).
❖ Additionally, the presence of molybdenum as a higher atomic number (or mass) compared to chromium in both lead compounds ($PbCrO_4$ and $PbMoO_4$) gave varied EBF values at the same applied energy (0.02 MeV) in the first stage of changing, while exposure to 1 MeV gave semi-identical numeric EBF values as a second

stage. The second stage gave a higher EBF value that may be related to the presence of the (Pb^{2+}) cation (esp. atomic number) compared to calcium molybdate.

❖ These tested ABO_4 molecules have a tetrahedral structure containing (Cr^{6+}, Mo^{6+}, or W^{6+}) ions linked to four oxygen atoms to form the BO_4^{2-} anion and neutralized by the charge of the cation (Pb^{2+} or Ca^{2+}) having a distorted hexahedral structure (i.e., $CaWO_4$ in Figure 9). Here, similarity in molecular structure was not an essential parameter for comparison, but it improved that the presence of a high mean atomic number in the anion or cation contributed to increasing gamma shielding properties. As suggested by the explanations of the tested materials at low energy exposure, the controlled parameter may be associated with the anion properties, while at higher energy exposure, the controlled factor was cation properties, especially atomic number (Table 7, Figure 10).
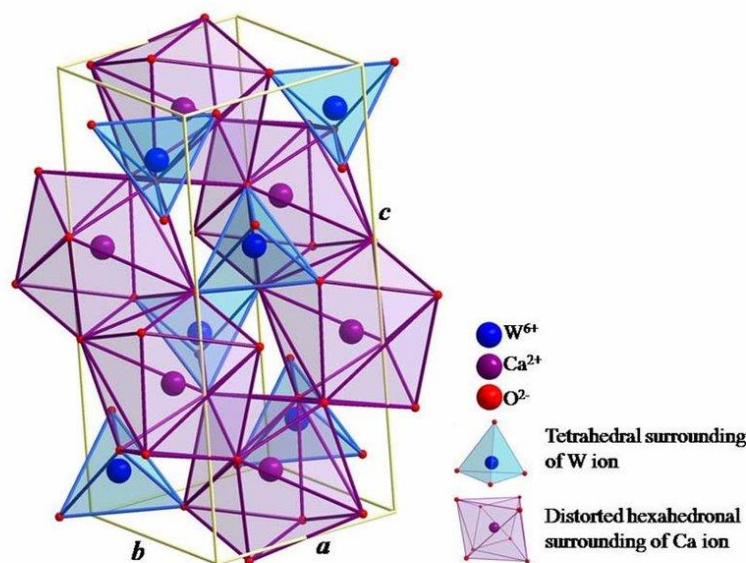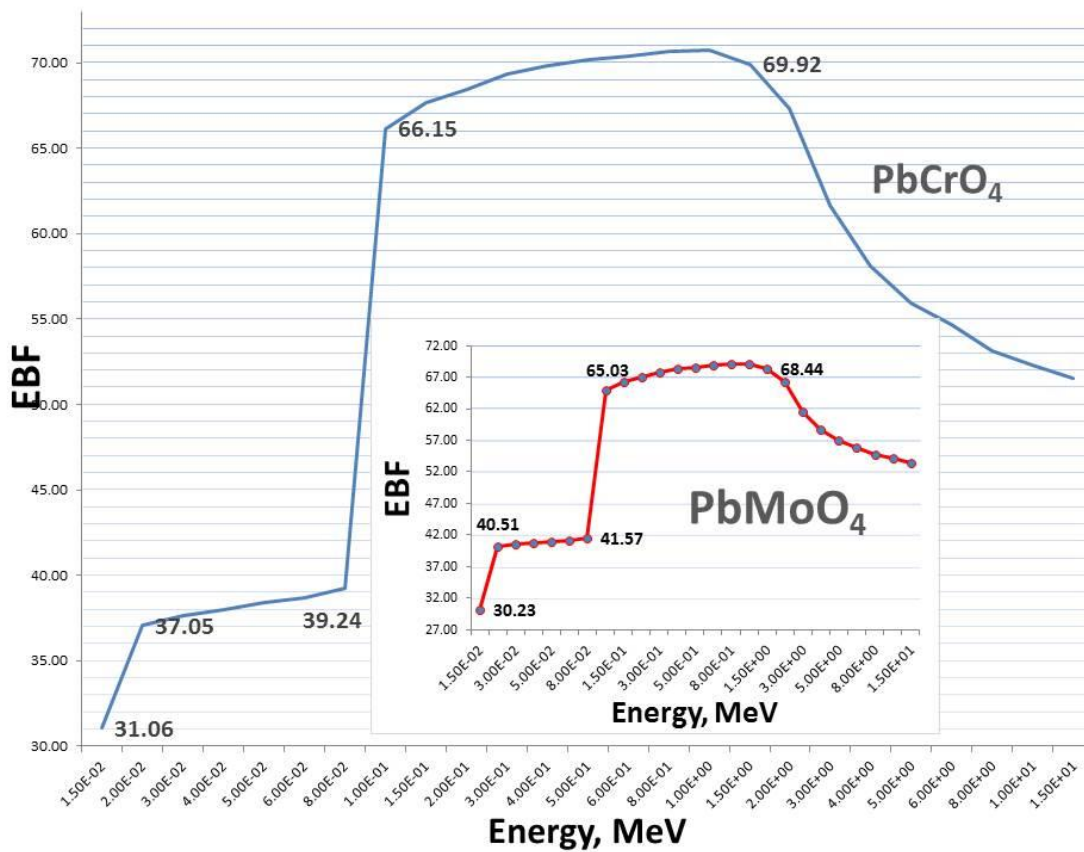

Figure (9). Molecular structure of $CaWO_4$ [31].

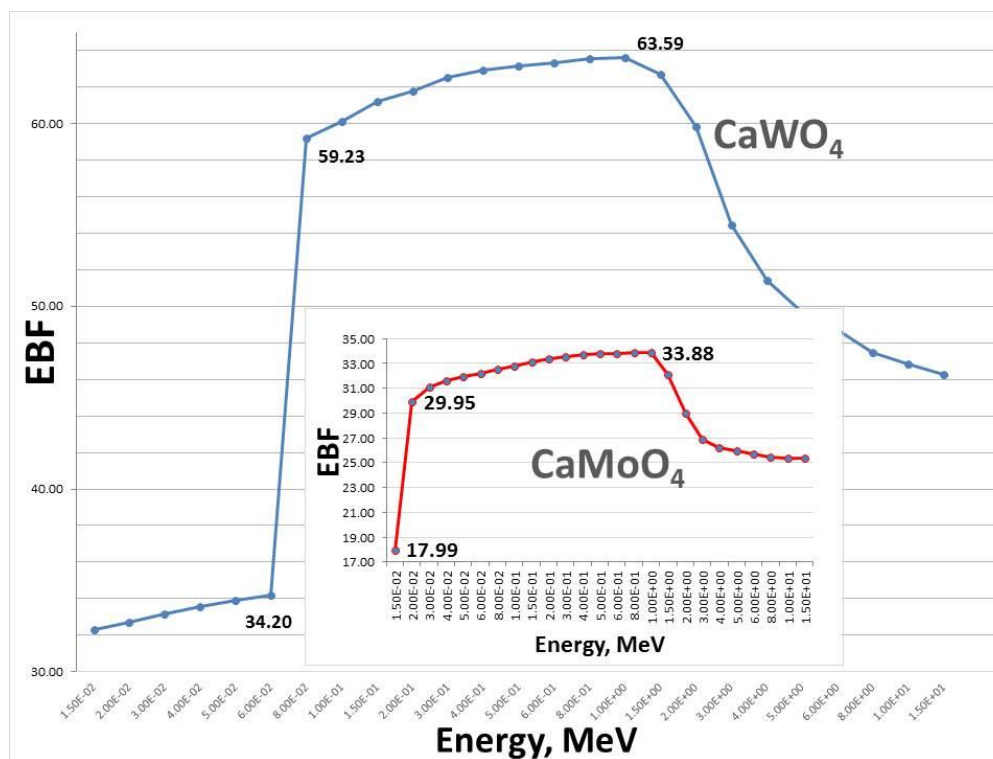**Figure (10a):** Variation between tested Lead oxyanion complexes showing two stages.

Figure (10b): Variation between tested Calcium oxyanion complexes showing one stage.

Table (7): Summary comparison between Z_{eq} values of the tested materials.

Energy, MeV	PbCrO$_4$	PbMoO$_4$	CaMoO$_4$	CaWO$_4$
1.50E-02	31.06	30.23	17.99	32.33
2.00E-02	37.05	40.22	29.95	32.71
8.00E-02	39.24	41.57	32.54	59.23
1.00E-01	66.15	65.03	32.77	60.10
1.00E+00	70.74	69.18	33.88	63.59

The exposure buildup factor curves at low energy initially increased to the maximum, and then, after several points, each curve sharply decreased at a specific point with increasing energy. Material performance at low energy is known as the Compton Effect. Table 7 shows this scattering at (0.02 or 0.08) MeV depending on the molecular composition and density.

5. Conclusions

Testing of new gamma shielding materials was performed by applying the Phy-X computerized-based method with ternary chromate, tungastate and molybdate having ABO_4 molecular formulas where (A = Ca or Pb and B = Mo, Cr, or W). Mass attenuation coefficients(μ_m) decreased exponentially with increasing photon energy in the low-energy region and then sharply decreased. Lead molybdate $PbMoO_4$ had the highest(μ_m) value, followed by $PbCrO_4$, $CaWO_4$, and $CaMoO_4$, which was related to the decrease in mean atomic numbers and densities. The mean free path (MFP) values decreased in the order of $PbMoO_4$, $PbCrO_4$, $CaWO_4$, and $CaMoO_4$ in reverse µm results due to the interaction between photons and the medium, indicating superior shielding properties where the MFP did not depend on the density. The HVL values of all samples increased with increasing incident photon energy, where the minimum HVL was detected in the presence of lead (Pb) due to the photoelectric effect that depends on the mean atomic number ($\overline{Z}$), while the maximum value had the lowest atomic number. The effective atomic number (Z_{eff}) decreased with decreasing mean atomic number and density, where $PbMoO_4$ had the highest value among the oxyanion complexes, indicating the highest γ-ray shielding capability. The dimensionless exposure buildup factor (EBF) reflects photon interference by calcium compounds compared to lead compounds, where atomic number (or mass) in addition to variation in density controls the shape and the resulting data. As a suggested explanation, the anion and cation properties, particularly the atomic number, of the ternary ABO_4 materials under testing were the controlled parameters at low and high energy exposure, respectively. From these four materials, $PbMoO_4$ was the best gamma shielding material with the needed qualifications in this important radiation safety subject.

Conflict of Interest: The authors declare that there are no conflicts of interest associated with this research project. We have no financial or personal relationships that could potentially bias our work or influence the interpretation of the results.

References

[1] T. Kaur, J. Sharma, and T. Singh, "Review on scope of metallic alloys in gamma rays shield designing," *Progress in Nuclear Energy*, vol. 113, pp. 95-113, 2019.

[2] Y. Chen and B. Yan, "The technology of shielding design for nuclear reactor: A review," *Progress in Nuclear Energy*, vol. 161, Article number 104741, 2023.

[3] I. Akkurt, C. Basyigit, S. Kilincarslan, B. Mavi, and A. Akkurt, "Radiation shielding of concretes containing different aggregates," *Cement and Concrete Composites*, vol. 28, no. 2, pp. 153-157, 2006.

[4] J. Kaewkhao, J. Laopaiboon, W. Chewpraditkul, "Determination of effective atomic numbers and effective electron densities for Cu/Zn alloy," *Journal of Quantitative Spectroscopy and Radiative Transfer,* vol. 109, no. 7, pp. 1260-1265, 2008.

[5] O. İçelli, S. Erzeneoğlu, İ. Karahan, and G. Çankaya, "Effective atomic numbers for CoCuNi alloys using

transmission experiments," *Journal of Quantitative Spectroscopy and Radiative Transfer,* vol. 91, no. 4, pp. 485-491, 2005.

[6] B. Alshahrani, I. Olarinoye, C. Mutuwong, C. Sriwunkum, H. Yakout , H. Tekin, M. Al-Buriahi, "Amorphous alloys with high Fe content for radiation shielding applications," *Radiation Physics and Chemistry,* vol. 183, Article number 109386, 2021.

[7] M. Aygun, Z. Aygun, and E. Ercan, "Radiation protection efficiency of newly produced W-based alloys: Experimental and computational study," *Radiation Physics and Chemistry,* vol. 212, Article number 111147, 2023.

[8] A. Acevedo-Del-Castillo, E. Águila-Toledo, S. Maldonado-Magnere, H. Aguilar-Bolados, "A Brief Review on the High-Energy Electromagnetic Radiation-Shielding Materials Based on Polymer Nanocomposites," *International Journal of Molecular Sciences,* vol. 22, no. 16, Article number 9079, 2021.

[9] S. Jadiyappa, "Radioisotope: Applications, Effects, and Occupational Protection, in Principles and Applications in Nuclear Engineering - Radiation Effects, Thermal Hydraulics, Radionuclide Migration in the Environment," R. Abdel Rahman and H. Saleh (Editors), InTech, UK, 2018.

[10] M. Abbas, A. El-Khatib, M. Elsafi, S. El-Shimy, M. Dib, H. Abdellatif, R. Baharoon, and M. Gouda, "Investigation of Gamma-Ray Shielding Properties of Bismuth Oxide Nanoparticles with a Bentonite–Gypsum Matrix," *Materials,* vol. 16, no. 5, Article number 2056, 2023.

[11] G. Lakshminarayana, M. Dong, M. Al-Buriahi, N. Rekik, D. Lee, J. Yoon, and T. Park, "Physical, structural, thermal, and mechanical features combined with neutron and gamma radiation attenuation qualities of Sm_2O_3 doped transparent borate-rich glasses," *Journal of Materials Research and Technology,* vol. 22, pp. 1268-1296, 2023.

[12] M. Sayyed, M. AlZaatreh, K. Matori, H. Sidek, and M. Zaid, "Comprehensive study on estimation of gamma-ray exposure buildup factors for smart polymers as a potent application in nuclear industries," *Results in Physics,* vol. 9, pp. 585-592, 2018.

[13] R. Lokhande, C. More, B. Surung, and P. Pawar, "Determination of attenuation parameters and energy absorption build-up factor of amine group materials," *Radiation Physics and Chemistry,* vol. 141, pp. 292-299, 2017.

[14] S. Kolavekara, G. Hiremath, P. Patil, N. Badigerb, and N. Ayachit, "Investigation of gamma-ray shielding parameters of bismuth phospho-tellurite glasses doped with varying Sm2O3," *Heliyon,* vol. 8, e11788 (9 pages), 2022.

[15] A. Taqi, A. Salih, and A. Ibrahim, "Electromagnetic-Ray Absorption Using B2O3-PbO-Na2O Glass Mixtures as Radiation Protection Shield," *Arab Journal of Nuclear Sciences and Applications,* vol. 55, no. 1 pp. 53 – 61, 2022.

[16] M. Yılmaz and F. Akman, "Gamma radiation shielding properties for polymer composites reinforced with bismuth tungstate in different proportions," *Applied Radiation and Isotopes,* vol. 200, Article number 110994, 2023.

[17] K. Mann, A. Rani, and M. Heer, "Shielding behaviors of some polymer and plastic materials for gamma-rays," *Radiation Physics and Chemistry,* vol. 106, pp. 247-254, 2015.

[18] M. Sayyed, H. Tekin, O. Kılıcoglu, O. Agar, and M. Zaid, "Shielding features of concrete types containing sepiolite mineral: Comprehensive study on experimental, XCOM and MCNPX results," *Results in Physics,* vol. 11, pp. 40-45, 2018.

[19] F. Akman, Z. Khattari, M. Kaçal, M. Sayyed, and F. Afaneh, "The radiation shielding features for some silicide, boride and oxide types ceramics,*" Radiation Physics and Chemistry*, vol. 160, pp. 9-14, 2019.

[20] G. Knoll. "Radiation Detection Measurement," 3rd Edition, John Wiley and Sons, USA, 2000.

[21] H. Özdemir and B. Camgöz, "Gamma radiation shielding effectiveness of cellular woven fabrics," *Journal of Industrial Textiles,* vol. 47, no. 5, pp. 712 – 726, 2018.

[22] D. Ochbclagh and S. Azimkhani, "Investigation of Gamma Ray Shielding Properties of Concrete Containing Different Percentages of Lead," *Applied Radiation and Isotopes,* vol. 70, no. 10, pp. 2282 - 2286, 2012.

[23] Q. Chang, S. Guo, and X. Zhang, "Radiation shielding polymer composites: Ray-interaction mechanism, structural design, manufacture and biomedical applications," *Materials and Design,* vol. 233, Article number 112253, 2023.

[24] L. Al-Ani, "Study of the Buildup Factor in Different Materials" M.Sc thesis, Department of Physics, College of Science, Baghdad University, Baghdad, Iraq, 1989.

[25] K. Hattif, "Gamma Ray Buildup Factor Measurement in Different Material," Ph.D thesis, Department of Physics, College of Science, Baghdad University, Baghdad, Iraq, 1994.

[26] H. Al-Ammar, "Studying the Buildup Factor and Angular Distribution of Gamma Rays in Multi-Layer Shields," M.Sc thesis, Department of Physics, College of Science, Baghdad University, Baghdad, Iraq, 1996.

[27] A. Al-Rawi, "Monte Carlo Method Calculation for Buildup Factor in Different Materials," M.Sc thesis, Department of Physics, College of Science, Al-Nahrain University, Baghdad, Iraq, 2003.

[28] M. Mahdi, "Simulation of Dose Buildup Factor of Gamma Ray Including Annihilation Radiation for Aluminum, Iron and Lead," M.Sc thesis, Department of Physics, College of Science, Al-Nahrain University, Baghdad, Iraq, 2014.

[29] H. Jawad, "A Study of Gamma Ray Dose Buildup Factors in Water and Graphite, in the Energy Range (4-10) MeV," M.Sc thesis, Department of Physics, College of Science, Al-Nahrain University, Baghdad, Iraq, 2017.

[30] X. Yan-Ling, Z. Hong, W. Rui, and Z. Chun-Yu, "Green Upconversion Luminescence in Er3+/Yb3+ Codoped CaWO4 Polycrystals," *Chinese Physics Letters,* vol. 28, no. 6, Article number 64210, 2011.

[31] C. Tablero, "Optical absorption and applications of the ABO4 (A = Ca, Pb and B = Mo, W) semiconductors," *Chemical Physics Letters,* vol. 635, pp. 190 -195, 2015.